LETTER

Mid–infrared frequency comb based on a quantum cascade laser

Andreas Hugi[1], Gustavo Villares[1], Stéphane Blaser[2], H. C. Liu[3] & Jérôme Faist[1]

Optical frequency combs[1] act as rulers in the frequency domain and have opened new avenues in many fields such as fundamental time metrology, spectroscopy and frequency synthesis. In particular, spectroscopy by means of optical frequency combs has surpassed the precision and speed of Fourier spectrometers. Such a spectroscopy technique is especially relevant for the mid-infrared range, where the fundamental rotational–vibrational bands of most light molecules are found[2]. Most mid-infrared comb sources are based on down-conversion of near-infrared, mode-locked, ultrafast lasers using nonlinear crystals[3]. Their use in frequency comb spectroscopy applications has resulted in an unequalled combination of spectral coverage, resolution and sensitivity[4–7]. Another means of comb generation is pumping an ultrahigh-quality factor microresonator with a continuous-wave laser[8–10]. However, these combs depend on a chain of optical components, which limits their use. Therefore, to widen the spectroscopic applications of such mid-infrared combs, a more direct and compact generation scheme, using electrical injection, is preferable. Here we present a compact, broadband, semiconductor frequency comb generator that operates in the mid-infrared. We demonstrate that the modes of a continuous-wave, free-running, broadband quantum cascade laser[11] are phase-locked. Combining mode proliferation based on four-wave mixing with gain provided by the quantum cascade laser leads to a phase relation similar to that of a frequency-modulated laser. The comb centre carrier wavelength is 7 micrometres. We identify a narrow drive current range with intermode beat linewidths narrower than 10 hertz. We find comb bandwidths of 4.4 per cent with an intermode stability of less than or equal to 200 hertz. The intermode beat can be varied over a frequency range of 65 kilohertz by radio-frequency injection. The large gain bandwidth and independent control over the carrier frequency offset and the mode spacing open the way to broadband, compact, all-solid-state mid-infrared spectrometers.

Unlike the situation in interband semiconductor lasers[12], mode-locked operation of typical high-performance, room-temperature quantum cascade lasers with emission of short single pulses is difficult to achieve because the gain recovery time ($\tau \approx 0.3\,\mathrm{ps}$) is much shorter than the time required by the pulse to complete one round-trip in the cavity (the round-trip time, $\tau_{rt} = 64\,\mathrm{ps}$), which defines the mode spacing. Such pulsed operation has so far only been achieved at cryogenic temperatures[13] over a locking bandwidth of 15 cm^{-1} at 77 K by incorporating an active region that used a diagonal transition with a very long upper-state lifetime[14]. Similarly, mode locking of ten modes has also been achieved at cryogenic temperature in terahertz quantum cascade lasers[15]. It should be noted, however, that the only requirement for comb operation in spectroscopy applications is the periodicity of the waveform at the round-trip frequency, not the generation of high-intensity pulses. Even though microcavity-based frequency combs have shown 'true' comb operation with millihertz stability, their output is sometimes nearly unmodulated in time[16,17]. In fact, because the intensity of a perfectly frequency-modulated laser is constant, the

power envelope of such a beam would not be perturbed by the fast gain recovery of the quantum cascade laser and the spectrum of such a laser would also be composed of equally spaced and discrete spectral lines. Furthermore, as in radio communication, a frequency-modulated signal may be more robust to noise than an amplitude-modulated signal. In addition, a constant output power can be preferable for linear spectroscopy applications, to avoid additional complexities caused by nonlinear interactions.

Nonlinear effects in quantum cascade lasers, triggering the onset of multimode operation, have been studied in detail[18]. As in interband lasers[19], spatial hole burning was found to have a key role in the onset of multimode instabilities. Two counterpropagating waves at frequencies ω_1 and ω_2 create a grating that beats at a frequency $\delta\omega = \omega_1 - \omega_2$, transferring energy between modes separated by that frequency difference. This gain mechanism is phase sensitive. In addition, intersubband transitions feature strong third-order optical nonlinearities, $\chi^{(3)}$, due to the large optical matrix element between the excited state and the empty lower states[20–22], allowing parametric processes due to four-wave mixing. It is important to stress that because these processes are quasi-resonant, the coupling between the modes will occur with a non-trivial phase delay. As shown schematically in Fig. 1a, the result of
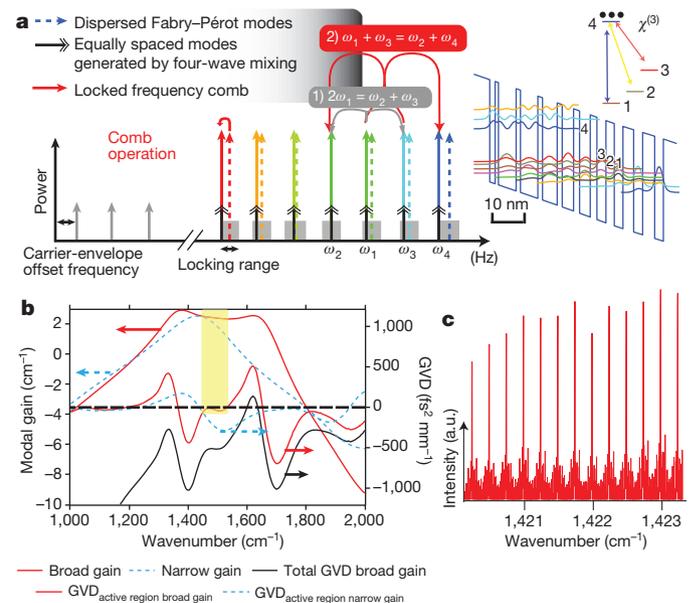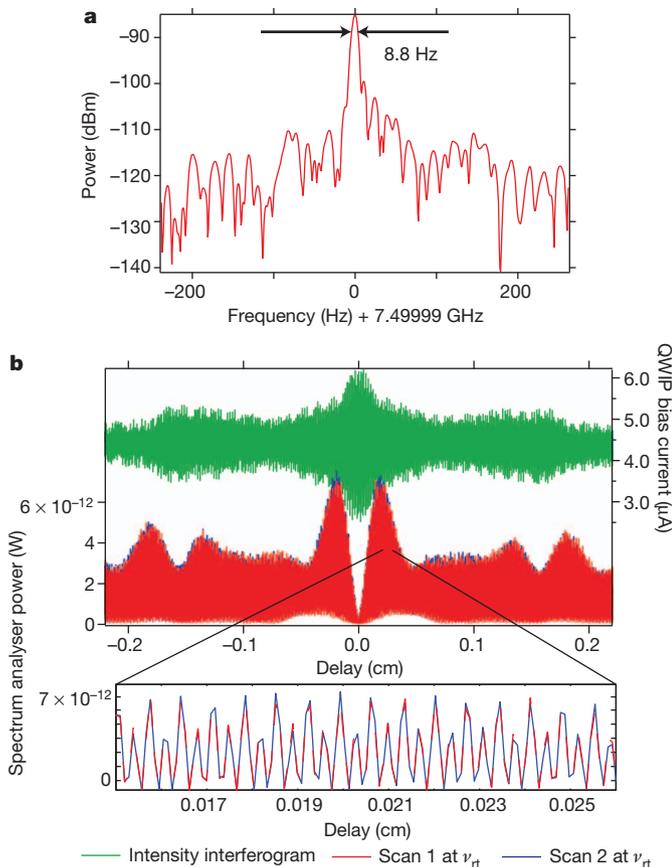

Figure 1 | Optical frequency comb in a quantum cascade laser. a, The dispersed Fabry–Pérot resonator modes lock to the equally spaced modes generated by four-wave mixing processes. **b,** Gain and GVD simulations of a narrowband (dotted) and a broadband (solid lines) quantum cascade laser. **c,** Magnified view of the laser spectra at $I = 740\,\mathrm{mA}$, measured using a high-resolution Fourier transform infrared spectrometer (0.0026 cm^{-1}, 78 MHz). a.u., arbitrary units.

[1]Institute for Quantum Electronics, ETH Zurich, 8093 Zurich, Switzerland. [2]Alpes Lasers SA, 1–3 Maximilien-de-Meuron, 2001 Neuchâtel, Switzerland. [3]Key Laboratory of Artificial Structures and Quantum Control, Department of Physics, Shanghai Jiao Tong University, Shanghai 200240, China.

these nonlinearities will be a proliferation of modes due to degenerate and non-degenerate four-wave mixing processes, in a similar fashion to what occurs in microcavity resonators[10].

The ability to lock longitudinal modes is limited by the material group velocity dispersion (GVD). Our heterogeneous quantum cascade laser is expected to have a much lower GVD in comparison with conventional devices[23]. It operates close to the zero-GVD point of our device, a InGaAs/InAlAs heterostructure grown on InP; the low doping of the active region and the waveguide design decrease the contribution from these components. In addition, as shown in Fig. 1b, and in contrast to conventional quantum cascade lasers, the computed GVD has a broad minimum in the centre of the gain curve owing to the 'flat top' shape of the gain curve of the broadband laser.
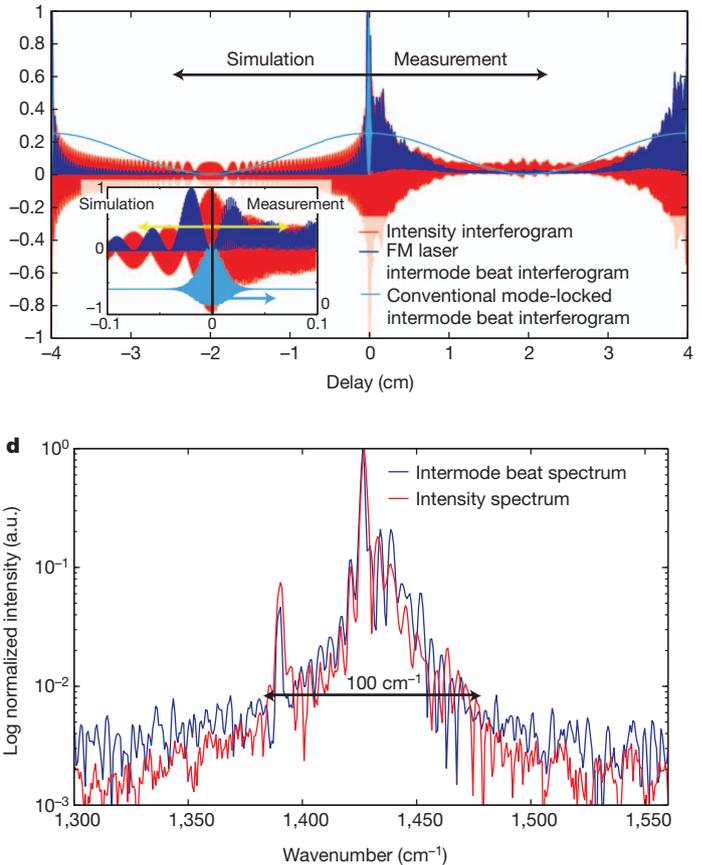
The broadband quantum cascade laser used in this work was composed of three different substacks and operated at a wavelength of around 7 μm. The laser spectra partly displayed in Fig. 1c were measured using a high-resolution Fourier transform infrared spectrometer and show a single set of longitudinal modes extending over 1.1 μm, with no measurable dispersion within the resolution ($0.0026\,\mathrm{cm}^{-1}$, 78 MHz) of the spectrometer over the whole dynamic range (Supplementary Fig. 1). All instabilities related to multiple transverse modes can be completely neglected. A selected set of spectra indicating the power per mode (between 1 μW and 3 mW) is displayed in Supplementary Fig. 2a. The total output power as a function of current at −20 °C is shown in Supplementary Fig. 2b. The device switches to multimode operation at $I = 460$ mA, shortly above threshold ($I_{\mathrm{th}} = 400$ mA). The spectrum, which is initially spread over $\delta\omega = 40\,\mathrm{cm}^{-1}$, broadens progressively to $\delta\omega = 230\,\mathrm{cm}^{-1}$ at the maximum current.

To investigate to what extent the modes are coupled, we first measure the intermode beat, that is, the radio-frequency spectrum of the intensity near the round-trip frequency, v_{rt}, using a fast quantum-well infrared photodetector[24]. Uncoupled modes (such as those originating from two free-running lasers driven in a similar way to our device) would generate a spectrum with a 5–10-MHz linewidth[25]. In contrast, as shown in Fig. 2a, such a measurement performed just above the onset of multimode operation shows a linewidth with a full-width at half-maximum of only $\delta v = 8.8$ Hz. For this current, the spectrum is already $\delta\omega = 15\,\mathrm{cm}^{-1}$ wide and contains 60 modes. This very narrow intermode beat is observed over the current range $I \approx 460$–480 mA. At higher temperatures (13 °C), this regime is more dominant and the comb spans up to $60\,\mathrm{cm}^{-1}$ (240 modes) with an intermode beat linewidth of $\leq$200 Hz. At a current of $\geq$480 mA, the intermode beat abruptly becomes wider: $\delta v \approx 48$ kHz. The intensity of the modulation of the laser output is never greater than 2%, indicating a mostly constant amplitude. The abrupt change in intermode beat linewidth is also reflected in the amplitude noise spectra shown in Supplementary Fig. 3. When the current is increased to 500 mA, the spectrum spans $\sim$100 cm^{-1} and the intermode beat widens to $\delta v < 250$ kHz. Above 510 mA, the single narrow intermode beat splits into two distinct broadened peaks spaced by 14 MHz.

The assessment of the coherence properties of a mode-locked laser is usually performed by an autocorrelation measurement on a nonlinear crystal to reveal the time structure of the optical pulse. This technique cannot be used in our case, because we do not expect the respective phases of the longitudinal modes to yield a single optical pulse with high peak intensity, suitable for nonlinear optics. To gain

Figure 2 | Intermode beat spectroscopy. a, Narrow intermode beat, with a full-width at half-maximum of <10 Hz at the onset of the multimode emission. The resolution bandwidth of the spectrum analyser is set to 10 Hz. **b**, Intensity interferogram and intermode beat interferograms measured in two successive scans separated by 90 min, at 490 mA. The resolution bandwidth is 100 kHz. QWIP, Quantum-well infrared photodetector. **c**, Comparison of the measured intermode beat interferogram at 480 mA with two intermode beat interferogram simulations of a perfectly frequency-modulated (FM) signal and a fundamentally mode-locked laser. Inset, magnified view of region at zero delay. **d**, Comparison of the intermode beat spectrum, $\mathcal{J}(v_{\mathrm{rt}},\omega)$, and the intensity spectrum, $\mathcal{J}(0,\omega)$, at an injection current of 500 mA.

insight into the respective phases and coherence properties of the modes, we present here an interferometric technique whereby the autocorrelation of the intermode beat is measured using a Michelson interferometer. The quantity measured is

$$I(v,\tau) = \left| \mathcal{F}\left(|E(t) + E(t+\tau)|^2 \right) \right| \qquad (1)$$

which is the absolute value of the Fourier component of the intensity at the detector at frequency v over a chosen resolution bandwidth of the spectrum analyser. Here E denotes the time-dependent amplitude of the electric field and $\mathcal{F}$ stands for the Fourier transform that is applied to the resulting intensity. The normal intensity interferogram measured in a Fourier transform infrared spectrometer is $I(0,\tau)$. In contrast to the intensity interferogram, the intermode beat interferogram, $I(v_{rt},\tau)$, is a function of both the amplitude and the relative phase of the modes. Furthermore, in analogy with Fourier spectroscopy, the Fourier transform

$$\mathcal{J}(v_{rt},\omega) = \mathcal{F}(I(v_{rt},\tau)) \qquad (2)$$

will yield the intermode beat spectrum, which roughly indicates the spectral regions contributing to the intermode beat.

Figure 2b shows two successive scans of $I(v_{rt},\tau)$ acquired with a resolution bandwidth of 100 kHz at the round-trip frequency, measured at 90-min intervals and an injection current of 490 mA. These scans (blue and red) are compared with the zero-frequency component $I(0,\tau)$ (green). Randomly varying phases would generate an intermode beat interferogram roughly proportional to the zero-frequency component around zero time delay (Supplementary Fig. 4). In contrast, the measured $I(v_{rt},\tau)$ shows long-term stability with a minimum at zero time delay, proving that there is a well-defined phase relation between the modes. The phase relation cannot be easily inferred from the measurement of $I(v_{rt},\tau)$, however. To help us do so, we compare the measured $I(v_{rt},\tau)$ to the respective signals predicted for a purely frequency-modulated signal and a conventional mode-locked laser (Fig. 2c; see Supplementary Fig. 5 for a measurement of an intermode beat interferogram of a mode-locked fibre laser). The phases are such that the amplitude modulation of the signal is strongly damped at zero delay ($\tau = 0$), as it would be for a frequency-modulated laser. In general, the comparison emphasizes the frequency modulation characteristics of the output of the laser, as expected from the short lifetime of the excited state. A minimum of the intermode beat is always

observed for $\tau = 0$ over all injected currents, indicating that the device never produces single pulses. To confirm further the frequency-modulated nature of the laser, we put a sheet of polyethylene, which has strong wavelength-dependent absorption, between the laser and the detector. This sheet acts as an optical discriminator that can convert the frequency modulation of the laser output to an amplitude modulation signal. As expected from a frequency-modulated signal, we find that the amplitude of the intermode beat at the detector increases. This amplification factor was measured to be 10–18.

The intermode beat spectrum, $\mathcal{J}(v_{rt},\omega)$, and the intensity spectrum, $\mathcal{J}(0,\omega)$, are compared in Fig. 2d and show that the entire laser spectrum contributes to the intermode beat. Regardless of the kilohertz intermode beat linewidth, we have a comb-like spectrum because the mode spacing does not fluctuate more than the chosen resolution bandwidth of the spectrum analyser over the whole laser spectrum. The measurement of the whole radio-frequency spectrum around v_{rt} as a function of τ yields important information about the mechanisms that destabilize the comb. An example of such characteristics is shown in Supplementary Fig. 6a at a high current ($I = 679$ mA) where the intermode beat has two peaks and a wide radio-frequency spectrum. By further increasing the size of the region with low GVD, it should be straightforward to increase the comb bandwidth.

To characterize the comb further, we did a heterodyne beat experiment between a comb line and a single-mode distributed-feedback quantum cascade laser (Supplementary Fig. 7a). The inset of Fig. 3a shows the spectrum of the single-mode quantum cascade laser alongside the comb spectrum that covers 60 cm^{-1} and has an intermode beat linewidth of $\leq$200 Hz. Figure 3a shows the corresponding heterodyne signal. A narrow linewidth of 1.3 MHz is measured, which simply reflects the temperature and current stability of our set-up. The increased phase noise directly translates into a broader linewidth of about 20 MHz in comb-like spectra.

Our measurements show that the low GVD, as well as the existence of nonlinearities, tends to lock the modes together. This locking can also be enhanced through radio-frequency injection. Such injection locking has already been successfully applied to a terahertz quantum cascade laser, enabling the demonstration of pulsed mode-locked operation. In our experiment, a radio-frequency power of 11 dBm is injected close to the round-trip frequency of 7.5 GHz, with an estimated injection loss of -34.5 dB. The direct current is set to 494 mA. While
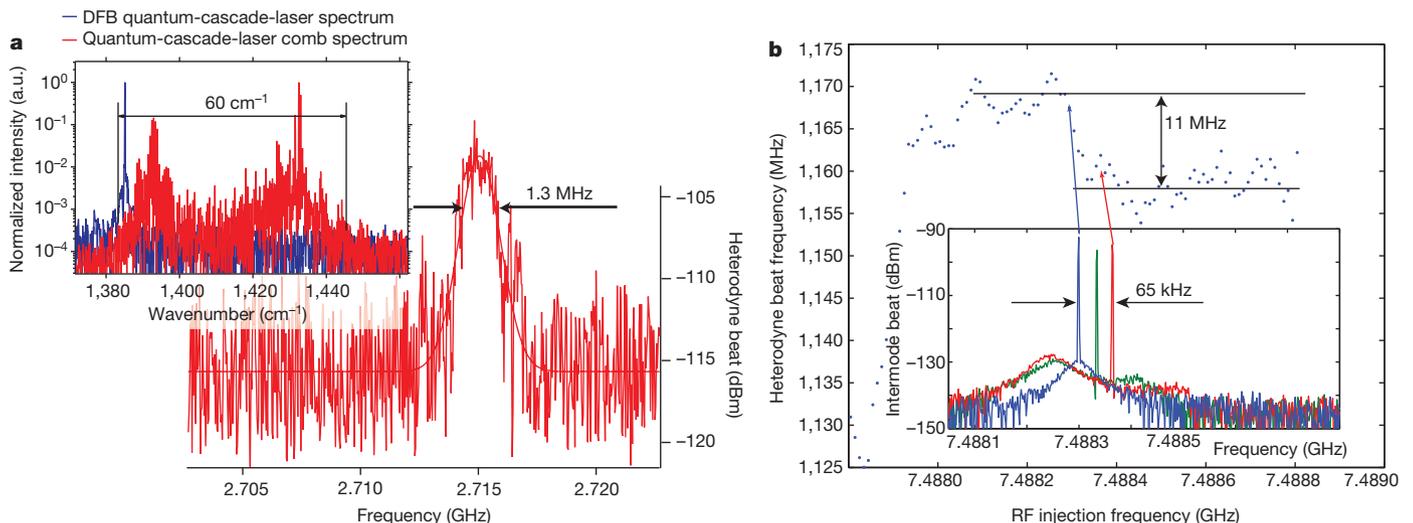
Figure 3 | Linewidth measurement and radio-frequency injection.
a, Heterodyne beat measurement between a single-mode distributed-feedback (DFB) quantum cascade laser and a quantum-cascade-laser comb line. The inset shows the two spectra. The measured heterodyne signal has a linewidth of 1.3 MHz. The resolution bandwidth is 500 kHz and the integration time is 25 ms. **b**, Heterodyne beat measurement of a comb-like line and a stable

single-mode quantum cascade laser while sweeping the radio-frequency (RF) injection frequency around the cavity round-trip frequency. When sweeping across the resonance of the cavity round-trip, the heterodyne signal can be shifted in frequency by 11 MHz. Inset, measured intermode beat at three different characteristic injection frequencies at resonance.

sweeping the radio frequency, we measure the heterodyne beat between one comb-like line and the single-mode quantum cascade laser (Supplementary Fig. 7a). Figure 3b shows the change in the heterodyne beat position and proves that we are able to change the mode spacing actively. The intermode beat with radio-frequency injection around resonance is shown in the inset of Fig. 3b. Unlike previous attempts[26], our measurements show the expected collapse of the intermode beat at the round-trip frequency to the resolution of the spectrum analyser. The round-trip frequency can be varied over a range of more than 65 kHz. There are approximately 167 modes between the peak of the laser and the mode that beats with the single-mode quantum cascade laser. Changing the round-trip frequency by 65 kHz should therefore result in a change of $167 \times 65\,\text{kHz} = 10.9\,\text{MHz}$ in the heterodyne beat signal, which agrees with the measured 11 MHz. It should be noted that the carrier frequency offset can be adjusted by the injected direct current (Supplementary Fig. 7b), whereas the mode spacing can be set through the radio-frequency injection. Therefore, it is possible to stabilize quantum-cascade-laser frequency combs fully[27]. However, as the injected radio-frequency power is increased to 26.6 dBm, the intermode beat interferogram resembles that of a fundamentally mode-locked laser, and, unlike the case for 11 dBm, the intermode beat spectrum shows that only a small fraction (18%) of the modes contribute to the injection-locked intermode beat (Supplementary Fig. 8).

We have presented a mid-infrared quantum-cascade-laser free-running optical frequency comb covering $60\,\text{cm}^{-1}$ (308 nm) at a centre wavenumber of $1{,}430\,\text{cm}^{-1}$ (7 μm). The measured linewidth of the comb lines is $\leq 1.3\,\text{MHz}$ with a narrow intermode beat linewidth of $\leq 200\,\text{Hz}$. At higher currents, we measure comb-like emission spectra that span $100\,\text{cm}^{-1}$ and have broader intermode beat linewidths (50–250 kHz). Further measurements using metrological techniques will give deeper insight into this system[28]. We have shown that the carrier-envelope offset frequency as well as the repetition frequency can be set independently by changing the direct current and through radio-frequency injection. The phase signature of the comb strongly resembles that of a frequency-modulated signal and is stable over time. We identify the locking mechanism responsible for the formation of the frequency comb to be four-wave mixing. Key physical properties of materials used in quantum cascade lasers in frequency combs are therefore strong third-order optical nonlinearities and a low GVD. Further investigation of the GVD and its sign is necessary[29]. Altogether, this system offers remarkable freedom of design, because it allows control over the electronic transitions, gain flatness, optical nonlinearities and dispersion through band structure engineering. The bandwidth of mid-infrared quantum-cascade-laser frequency combs can be improved through a detailed understanding of the phase-locking mechanism and by appropriately engineering the GVD using waveguide design and facet coatings. The large bandwidth, in combination with independent control over the carrier frequency offset and the mode spacing, opens the way to metrological and sensing applications. Thus, the mid-infrared quantum-cascade-laser frequency comb could become standard technology for broadband, compact, all-solid-state mid-infrared spectrometers.

METHODS SUMMARY

Calculation of the GVD. We include three contributions to the GVD in our calculations. First, the vertical and lateral modal GVDs of the guided mode (GVD_{vert} and GVD_{lat}). GVD_{vert} includes the dispersion of the doped layers due to free-carrier absorption and material dispersion. Second, the GVD due to the gain and loss in the active region. These produce a change in the refractive index, Δn_2, calculated through Kramers–Kronig relations. The gain is calculated using software based on a density matrix model extended to the whole structure, which also includes second-order gain and loss mechanism between all sub-band pairs[30]. The total losses are set to $2.5\,\text{cm}^{-1}$. Because the broadband active region is composed of three substacks, each individual stack is simulated again including the loss introduced through cross-absorption. This takes into account the inhomogeneous broadening of these devices. Third, we account for the GVD due to material

dispersion. The total GVD is calculated as a sum of the individual terms weighted by the modal overlap.

Intermode beat spectroscopy set-up. Supplementary Fig. 9 shows the intermode beat spectroscopy set-up. The laser light is collimated through an antireflection-coated ZnSe lens. The light passes through an antireflection-coated quarter-wave plate to reduce the effect of feedback originating from reflections from optical components. The light passes through a Fourier transform infrared spectrometer (Bruker IFS66/S) and is focused through an antireflection-coated ZnSe lens on a $80\,\text{μm} \times 80\,\text{μm}$ quantum-well infrared photodetector cooled to the temperature of liquid nitrogen. The Fourier transform infrared spectrometer is run in step-scan mode. At each step, we record the radio-frequency spectrum at the round-trip frequency of the laser. Concurrently, we record the intensity component of the interferogram through the bias current of the photodetector.

1. Udem, T., Holzwarth, R. & Hänsch, T. W. Optical frequency metrology. *Nature* **416,** 233–237 (2002).
2. Keilmann, F., Gohle, C. & Holzwarth, R. Time-domain mid-infrared frequency-comb spectrometer. *Opt. Lett.* **29,** 1542–1544 (2004).
3. Adler, F. et al. Phase-stabilized, 1.5 W frequency comb at 2.8–4.8 μm. *Opt. Lett.* **34,** 1330–1332 (2009).
4. Johnson, T. A. & Diddams, S. A. Mid-infrared upconversion spectroscopy based on a Yb:fiber femtosecond laser. *Appl. Phys. B* **107,** 31–39 (2012).
5. Foltynowicz, A., Ban, T., Masłowski, P., Adler, F. & Ye, J. Quantum-noise-limited optical frequency comb spectroscopy. *Phys. Rev. Lett.* **107,** 233002 (2011).
6. Adler, F., Thorpe, M. J., Cossel, K. C. & Ye, J. Cavity-enhanced direct frequency comb spectroscopy: technology and applications. *Annu. Rev. Anal. Chem.* **3,** 175–205 (2010).
7. Vodopyanov, K. L., Sorokin, E., Sorokina, I. T. & Schunemann, P. G. Mid-IR frequency comb source spanning 4.4–5.4 μm based on subharmonic GaAs optical parametric oscillator. *Opt. Lett.* **36,** 2275–2277 (2011).
8. Del'Haye, P. et al. Optical frequency comb generation from a monolithic microresonator. *Nature* **450,** 1214–1217 (2007).
9. Wang, C. Y. et al. Mid-infrared optical frequency combs based on crystalline microresonators. Preprint at http://arxiv.org/abs/1109.2716 (2011).
10. Kippenberg, T. J., Holzwarth, R. & Diddams, S. A. Microresonator-based optical frequency combs. *Science* **332,** 555–559 (2011).
11. Faist, J. et al. Quantum cascade laser. *Science* **264,** 553–556 (1994).
12. Derickson, D. J. et al. Short pulse generation using multisegment mode-locked semiconductor lasers. *IEEE J. Quantum Electron.* **28,** 2186–2202 (1992).
13. Wang, C. Y. et al. Mode-locked pulses from mid-infrared quantum cascade lasers. *Opt. Express* **17,** 12929–12943 (2009).
14. Faist, J. et al. Laser action by tuning the oscillator strength. *Nature* **387,** 777–782 (1997).
15. Barbieri, S. et al. Coherent sampling of active mode-locked terahertz quantum cascade lasers and frequency synthesis. *Nature Photon.* **5,** 306–313 (2011).
16. Del'Haye, P., Arcizet, O., Schliesser, A., Holzwarth, R. & Kippenberg, T. Full stabilization of a microresonator-based optical frequency comb. *Phys. Rev. Lett.* **101,** 053903 (2008).
17. Ferdous, F. et al. Spectral line-by-line pulse shaping of on-chip microresonator frequency combs. *Nature Photon.* **5,** 770–776 (2011).
18. Gordon, A. et al. Multimode regimes in quantum cascade lasers: from coherent instabilities to spatial hole burning. *Phys. Rev. A* **77,** 053804 (2008).
19. Yamada, M. Theoretical analysis of nonlinear optical phenomena taking into account the beating vibration of the electron density in semiconductor lasers. *J. Appl. Phys.* **66,** 81–89 (1989).
20. Walrod, D., Auyang, S. Y., Wolff, P. A. & Sugimoto, M. Observation of third order optical nonlinearity due to intersubband transitions in AlGaAs/GaAs superlattices. *Appl. Phys. Lett.* **59,** 2932–2934 (1991).
21. Rosencher, E. et al. Quantum engineering of optical nonlinearities. *Science* **271,** 168–173 (1996).
22. Banerjee, S. & Shore, K. A. MIR and NIR nonlinear optical processing using intersubband $\chi^{(3)}$ in triple quantum well structures. *Semicond. Sci. Technol.* **18,** 655–660 (2003).
23. Parz, W. et al. Intersubband gain-induced dispersion. *Opt. Lett.* **34,** 208–210 (2009).
24. Grant, P. D., Dudek, R., Buchanan, M. & Liu, H. C. Room-temperature heterodyne detection up to 110 GHz with a quantum-well infrared photodetector. *IEEE Photon. Technol. Lett.* **18,** 2218–2220 (2006).
25. Aellen, T. et al. Direct measurement of the linewidth enhancement factor by optical heterodyning of an amplitude-modulated quantum cascade laser. *Appl. Phys. Lett.* **89,** 091121 (2006).
26. Soibel, A. et al. Active mode locking of broadband quantum cascade lasers. *IEEE J. Quantum Electron.* **40,** 844–851 (2004).
27. Telle, H. et al. Carrier-envelope offset phase control: a novel concept for absolute optical frequency measurement and ultrashort pulse generation. *Appl. Phys. B* **69,** 327–332 (1999).
28. Braje, D., Hollberg, L. & Diddams, S. Brillouin-enhanced hyperparametric generation of an optical frequency comb in a monolithic highly nonlinear fiber cavity pumped by a cw laser. *Phys. Rev. Lett.* **102,** 193902 (2009).
29. Herr, T. et al. Universal formation dynamics and noise of Kerr-frequency combs in microresonators. *Nature Photon.* **6,** 480–487 (2012).

30. Terazzi, R. & Faist, J. A density matrix model of transport and radiation in quantum cascade lasers. *N. J. Phys.* **12,** 033045 (2010).

Author Contributions A.H. carried out the measurements. Simulations and ideas were developed by A.H. and J.F. G.V. contributed to the heterodyne beat measurements as well as the amplitude noise measurements. S.B. provided both quantum cascade lasers. H.C.L. provided the quantum-well infrared photodetector. All the work was done under the supervision of J.F.

Author Information Reprints and permissions information is available at www.nature.com/reprints. The authors declare no competing financial interests. Readers are welcome to comment on the online version of the paper. Correspondence and requests for materials should be addressed to J.F. (jfaist@ethz.ch) or H.C.L. (h.c.liu@sjtu.edu.cn).